2021 43rd Annual International Conference of the
IEEE Engineering in Medicine & Biology Society (EMBC)
Oct 31 - Nov 4, 2021. Virtual Conference

Spectral Features Based Decoding of Task Engagement: The Role of Theta and High Gamma Bands in Cognitive Control

Sandeep Avvaru, *Student Member*, *IEEE*, Nicole R. Provenza, Alik S. Widge, and Keshab K. Parhi, *Fellow*, *IEEE*

***Abstract*— This paper analyzes local field potentials (LFP) from 10 human subjects to discover frequency-dependent biomarkers of cognitive conflict. We utilize cortical and subcortical LFP recordings from the subjects during a cognitive task known as the Multi-Source Interference Task (MSIT). We decode the task engagement and discover biomarkers that may facilitate closed-loop neuromodulation to enhance cognitive control. First, we show that spectral power features in predefined frequency bands can be used to classify task and non-task segments with a median accuracy of 88.1%. Here the features are first ranked using the *Bayes Factor* and then used as inputs to subject-specific linear support vector machine classifiers. Second, we show that theta (4–8 Hz) band, and high gamma (65–200 Hz) band oscillations are modulated during the task performance. Third, by isolating time-series from specific brain regions of interest, we observe that a subset of the dorsolateral prefrontal cortex features is sufficient to decode the task states. The paper shows that cognitive control evokes robust neurological signatures, especially in the prefrontal cortex (PFC).**

I. Introduction

Neuropsychiatric disorders are the leading cause of disability in the United States; about one in every five American adults experiences mental illness. Existing treatments for mental illness are less than 50% effective, which calls for a better understanding of the mechanisms underlying these disorders that can lead to alleviation of impaired cognitive control. Electrical deep brain stimulation (DBS) has been shown to be promising, but it suffers from ambiguous clinical outcomes, which limit its usage [1]–[3]. The action mechanisms of DBS are still unclear, and several questions are yet to be answered: What should be the target stimulation site? What are the best stimulation parameters (e.g., current, frequency, and duty cycle)? Dysfunctional decision-making and cognitive control are common features in a wide range of mental disorders such as depression, addiction, anxiety disorders, autism spectrum disorders, schizophrenia, and obsessive-compulsive disorder (OCD) [4], [5]. Cognitive control involves restricting and controlling default responses in favor of a more desired adaptive response.

Developing an adaptive system that can calibrate stimulation in response to predefined biomarkers (for cognitive effort) may improve DBS efficacy, but this requires further knowledge about its neural signatures [6], [7]. A closed-loop direct brain stimulation strategy was developed in a recent study to enhance cognitive control [8]. However, it is still unclear when to automatically activate the intervention. Therefore, further research is necessary to discover the best biomarkers for cognitive control in humans. This paper attempts to uncover frequency-dependent biomarkers by classifying task engagement from background (non-task) activity. To this end, we utilize local field potential signals as ten subjects perform the Multi-Source Interference Task (MSIT), a well-established experimental paradigm to study cognitive control [9]. The MSIT has been shown to evoke connectivity changes related to cognitive impairment in major depressive disorder (MDD), OCD, and schizophrenia [10], [11]. A similar decoding of task activity based on fixed canonical correlation analysis was demonstrated in [12]. However, the canonical correlation operators are not readily implementable on an implanted device. The main advantage of this approach is that the proposed features make it feasible to develop, implement and evaluate an adaptive neuromodulation mechanism using existing hardware devices.

II. Materials and Methods

A. The Multi-Source Interference Task (MSIT)

In 2003, Bush et al. developed the Multi-Source Interference Task (MSIT) that reliably and robustly activates the cingulo-frontal-parietal (CFP) network in individual healthy subjects [9]. This network plays a crucial role in cognitive processing. Thus, the MSIT can discern cognition in healthy individuals and patients with neuropsychiatric disorders. These disorders include schizophrenia, attention deficit hyperactive disorder (ADHD), and obsessive-compulsive disorder (OCD). Subsequent experiments also showed that the MSIT performance is affected by electrical stimulation [8], [13]. The experimental setup, as depicted in Fig. 1(a), consisted of 1–5 blocks of trials. Each trial-block had 32 or 64 trials. The task stimuli in each trial comprised of an

The data were originally collected with support from the Defense Advanced Research Projects Agency (DARPA) under Cooperative Agreement Number W911NF-14-2-0045 issued by ARO contracting office in support of DARPA's SUBNETS Program. S. Avvaru was supported by the MNDrive Neuromodulation Research Fellowship. A.S. Widge acknowledges additional research support from the MNDrive Brain Conditions program, the UMN Medical Discovery Team on Addiction, and the National Institutes of Health (R01NS113804, R01MH123634). All views presented herein are those of the authors, not the policy of any government agency or other funding body.

This research was supported in part by the National Science Foundation under grant number CCF-1954749.

S. Avvaru and K. K. Parhi are with the Department of Electrical and Computer Engineering, University of Minnesota, Minneapolis, MN 55455, USA (email: avvar002@umn.edu and parhi@umn.edu).

N. R. Provenza is with Brown University School of Engineering, Providence, RI, USA

A. S. Widge is with the Department of Psychiatry and Behavioral Sciences, University of Minnesota, Minneapolis, MN 55455, USA

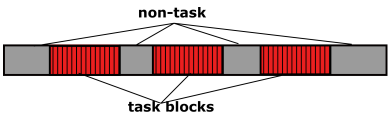

(a) Block structure of the MSIT trials

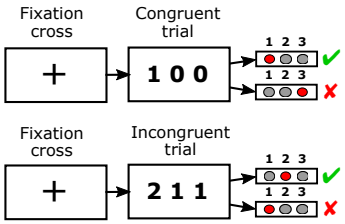

(b) Examples of congruent and incongruent trials

Fig. 1: The Multi-Source Interference Task.

array of three numbers (1, 2, or 3) presented at the center of a computer screen. The subjects were asked to report, via button press, the value of the unique number that differs from the other two distractors (see 1(b)). If the distractors were a '0' and the target's position matched its value, the trials were called *congruent* trials. Otherwise, they were referred to as *incongruent* trials. Each experimental run comprised a roughly equal number of congruent and incongruent trials. The incongruent trials were also characterized by a slightly lower success rate of $97.1 \pm 5.52\%$ compared to $100\% \pm 2.47\%$ associated with the congruent trials [12].

B. Data Description

Ten subjects with a history of drug-resistant epilepsy participated in the MSIT task as they were hospitalized for invasive epilepsy monitoring. According to the study sponsor guidelines, each participant gave fully informed consent. The local institutional review board approved all procedures at Partners Healthcare (Massachusetts General Hospital), and additional review occurred through the US Army Human Research Protection Office.

Local field potential (LFP) signals were recorded through depth electrodes surgically implanted for each participant's seizure monitoring. Between five and eight (nine) electrodes with diameters 0.8-1.0 mm were placed in the left (right) hemisphere. Each electrode consisted of 8-16 platinum/iridium contacts. The signals were acquired at a 2 kHz sampling rate via neural signal processor recording systems from Blackrock Microsystems Inc., Salt Lake City, UT. All signals were referenced to a scalp EEG electrode.

Electrodes with excessive line noise (60 Hz), close to seizure focus (based on clinical reports), and other artifacts found on visual inspection were removed. Each channel was down-sampled to 1000 Hz, followed by subtraction of the mean, and bandstop filtered to remove line noise at 60 Hz, 120 Hz, and 180 Hz. Adjacent channels were then bipolar re-referenced to each other to alleviate the effect of volume conduction [14]. The regions of interest were parcellated based on the Desikan-Killiany-Tourville brain atlas [15]. This data was reported in [12].

C. Features and Classification

1) Extracting task and non-task segments: The onset of the fixation cross marked the beginning of each trial. The trials lasted at least 3.8 s. Therefore, 3.8 s segments of neural recordings from the onset of each trial constitute *task data*. The recordings during the rest phase, i.e., before and after the task activity are considered *non-task data* (see Fig. 1(a)). Unbiased classification of the two mental states requires class-balancing. For subjects with insufficient non-task data, overlapping windows were used to create more segments.

2) Feature extraction and selection: Spectral powers in predefined frequency bands were used as features to differentiate between the two classes. Prior studies demonstrate that spectral power based features can distinguish psychiatric and neurological disorders [16]–[19]. Five frequency bands between 4 Hz and 200 Hz were considered. These bands are defined as follows: theta (4–8 Hz), alpha (8–13 Hz), beta (13–30 Hz), low gamma (30–55 Hz), and high gamma (65–200 Hz). Additionally, the total power (1–200 Hz) is also considered a feature. The spectral powers were computed as averaged periodogram estimates in the frequency bands using the Matlab function *bandpower*. Consequently, a subject with N channels has $6 \times N$ total features. The number of bipolar re-referenced channels ranged between 64 and 195 based on the subjects' electrode montage.

The features were then ranked using the Bayes factor. The Bayesian approach, unlike p-values, yields an intuitive interpretation of the evidence supported by data [20]. Although significant p-values can provide evidence against the null hypothesis, the inverse may not be true [21]. This ambiguity and lack of a formal calculus of inference make p-values elusive to interpret [22]. In contrast, the Bayes factor (sometimes referred to as *likelihood ratio*) measures the strength of relative evidence that the data provide for one hypothesis versus the other.

Consider two possible hypotheses H_0 and H_1 for a data. The evidence for the hypothesis can be compared by looking at the posterior odds Ω, which can be computed as,

$$\Omega = \frac{Pr(H_0|data)}{Pr(H1|data)} = \frac{Pr(data|H_0)}{Pr(data|H1)} \frac{Pr(H_0)}{Pr(H1)}$$

In practice, it is reasonable to set the prior odds $\frac{Pr(H_0)}{Pr(H_1)} = 1$, to be unbiased towards either hypotheses. The data in the two classes were balanced making this a reasonable assumption. This assumption reduces Ω to the ratio of *marginal likelihoods* $Pr(data|H_0)$ and $Pr(data|H_1)$. This ratio, known as the Bayes factor BF, is given by the equation,

$$BF = \frac{Pr(data|H_0)}{Pr(data|H_1)}.$$

The likelihoods were computed assuming the data in both classes are Gaussian.

III. Results

A. Classifier Performance

For each subject, the data were split into ten subsets via sequential sub-sampling to ensure that test samples are not in

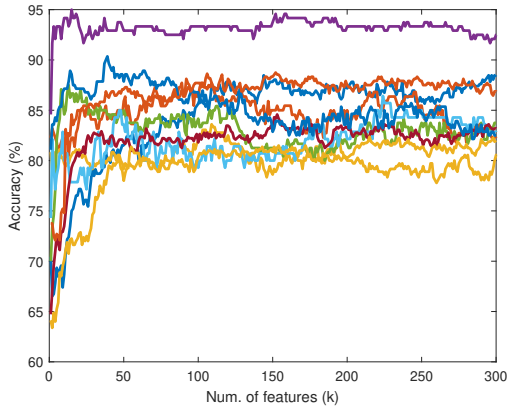

Fig. 2: Classification accuracy as a function of the number of features (k). The reported values are mean 10-fold cross-validation accuracy. Each plot represents a different subject.

the training samples' temporal vicinity. One of the ten folds acts as the test set in each iteration, while the other nine act as the training data. This procedure ensures that all the data are tested and makes the classifiers less prone to overfitting.

Classification accuracy of each of the ten test sets was computed using the top k features (ranked using Bayes factor) as inputs to linear support vector machine (SVM) classifiers. This process was repeated by changing the value of k up to a maximum of 600 features. The top k^* features with maximum accuracy are considered the *optimal features* for each subject. The median value of k^* was observed to be 184. Fig. 2 illustrates how the accuracy changes as a function of k till $k = 300$. It can be observed that the accuracy increases with the value of k. All subjects attain a near-maximum accuracy with 50 features, after which the improvement is marginal.

The best accuracy for the 10 subjects varied between 82.5% to 95%. The median classification accuracy is 88.1%, with a standard deviation of 3.7%. These results show that frequency-domain features can reliably distinguish task states from non-task states. The low standard deviation shows the robustness of the approach across multiple subjects. The task and non-task classification rates (sensitivity and specificity) are $90 \pm 4.7\%$ and $87 \pm 4.3\%$, respectively. These rates are significantly higher than a prior approach based on the fixed canonical correlation analysis (FCCA) for the same data [12].

B. The Role of Theta and High Gamma Bands

Prior studies show that specific frequency bands could be associated with cognitive control [13], [23], [23], [24]. To determine the contribution of each of the five bands, we categorize the optimal features into five groups based on their corresponding frequency bands. Let $\mathcal{F}$ be set of all available features for a given subject. The number of features in $\mathcal{F}$, i.e., $|\mathcal{F}|$ depends on the number of channels of signals recorded from the subject. The set of optimal features selected by the features selection method is denoted by $\mathcal{F}^*$, where $\mathcal{F}* \subset \mathcal{F}$. The proportion of optimal features (p) in a subband B is given by $p = |\mathcal{F}^*_{\mathcal{B}}|/|\mathcal{F}^*|$, where $\mathcal{F}^*_{\mathcal{B}} \subset \mathcal{F}^*$ is the set of optimal features corresponding to the frequency band B.

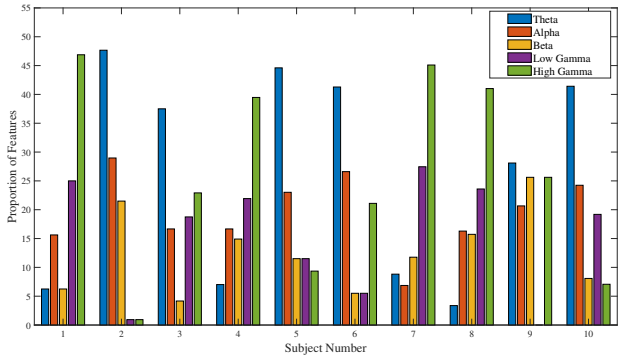

Fig. 3: Proportion of optimal features from a specific frequency band.

TABLE I: Summary of task vs. non-task classification results. Random label-assignment would result in a baseline accuracy of 50%

Features	FCCA [12]	Proposed–all reg.	Proposed–dlPFC
Accuracy	78.1	88.07	86.57
Sensitivity	71.0	90.05	86.97
Specificity	79.2	87	85.07

We observe that at least 40% of the optimal features originate from theta band (4–8 Hz) activity in six subjects. In the remaining four subjects, high gamma (65–200 Hz) is more involved. Fig. 3 presents the proportion of optimal features (p) in each of the five bands: theta, alpha, beta, low gamma, and high gamma. It shows that the theta (median $p = 32.8\%$) and the high gamma (median $p = 24.3\%$) bands play a dominant role in the MSIT task engagement.

C. Comparison of Regions

Next, we isolated the recordings from specific regions of interest. We observed each region's ability to decode task states. The ten regions of interest span across at least nine subjects: amygdala, caudate, dorsal anterior cingulate cortex, dorsolateral prefrontal cortex, dorsomedial prefrontal cortex, hippocampus, lateral orbitofrontal cortex, medial orbitofrontal cortex, temporal lobe, and ventrolateral prefrontal cortex. Fig. 4 shows a comparison of classifier performance of the ten regions of interest. The results illustrate that a subset of optimal features from one brain region can maintain the decoding ability. The dorsolateral PFC is the most contributory region in all ten subjects with a median classification accuracy of $86.6 \pm 5.2\%$. The number of features required to achieve the best accuracy was 115 (median of the ten subjects). We can attain an accuracy of 88.1% using all available regions (see Fig. 2), which is only marginally higher. The second and the third best decoding performances are from the temporal lobe and the dorsomedial PFC with median accuracies of 83.6% and 81.6%, respectively. The summary of prediction accuracies is presented in Table I.

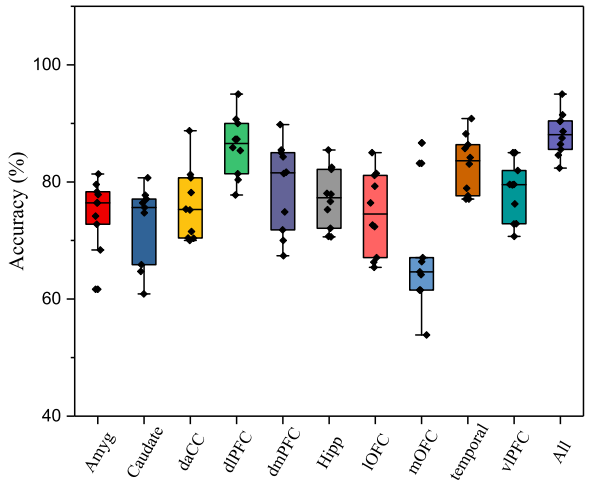

Fig. 4: Task vs. non-task classification accuracy using recordings from a specific region.

IV. Conclusion

Effective treatment of psychiatric diseases requires detecting cognitive control states, identifying lapses in control, and neurostimulation as patients go about their daily lives. The ability to differentiate task and non-task mental states with high accuracy, as demonstrated in this paper, is crucial to identify objective biomarkers of cognitive control. The cross-validation ensures that the results generalize across time, and the low standard deviation of 3.7% indicates the validity of the approach for multiple subjects. The discriminatory capacity of theta band (see Fig. 3) corroborates recent findings [23], [24]. Disorders such as schizophrenia and OCD have been linked to dysfunctional modulation in dlPFC [25], [26]. As shown in [27], [28], using dlPFC as a stimulation site may enhance cognitive control. The results in Fig. 4 validate the hypothesis that cognitive effort involves modulation of dlPFC. Additionally, the decoders presented here utilize spectral powers in pre-defined frequency bands, which can be computed using existing neuromodulation devices without a significant computational overhead.

References

[1] J. Massano and C. Garrett, "Deep brain stimulation and cognitive decline in parkinson's disease: A clinical review," *Frontiers in Neurology*, vol. 3, p. 66, 2012.

[2] A. S. Widge, D. A. Malone *et al.*, "Closing the loop on deep brain stimulation for treatment-resistant depression," *Frontiers in Neuroscience*, vol. 12, p. 175, 2018.

[3] A. Widge and D. Dougherty, "Deep brain stimulation for treatment-refractory mood and obsessive-compulsive disorders," *Current Behavioral Neuroscience Reports*, vol. 2, 08 2015.

[4] A. F. Arnsten and K. Rubia, "Neurobiological circuits regulating attention, cognitive control, motivation, and emotion: Disruptions in neurodevelopmental psychiatric disorders," *J. of the American Academy of Child & Adolescent Psychiatry*, vol. 51, no. 4, pp. 356 – 367, 2012.

[5] L. M. McTeague, J. Huemer *et al.*, "Identification of common neural circuit disruptions in cognitive control across psychiatric disorders," *American Journal of Psychiatry*, vol. 174, no. 7, pp. 676–685, 2017.

[6] N. Provenza, E. Matteson *et al.*, "The case for adaptive neuromodulation to treat severe intractable mental disorders," *Frontiers in Neuroscience*, vol. 13, 02 2019.

[7] A. S. Widge, K. K. Ellard *et al.*, "Treating refractory mental illness with closed-loop brain stimulation: Progress towards a patient-specific transdiagnostic approach," *Experimental Neurology*, vol. 287, pp. 461 – 472, 2017.

[8] I. Basu, A. Yousefi *et al.*, "Closed loop enhancement and neural decoding of human cognitive control," *bioRxiv*, 2020.

[9] G. Bush, L. Shin *et al.*, "The multi-source interference task: Validation study with fMRI in individual subjects," *Molecular psychiatry*, vol. 8, pp. 60–70, 01 2003.

[10] C. Davey, M. Yucel *et al.*, "Task-related deactivation and functional connectivity of the subgenual cingulate cortex in major depressive disorder," *Frontiers in psychiatry*, vol. 3, p. 14, 02 2012.

[11] S. Heckers, A. P. Weiss *et al.*, "Anterior cingulate cortex activation during cognitive interference in schizophrenia," *American Journal of Psychiatry*, vol. 161, no. 4, pp. 707–715, 2004, pMID: 15056518.

[12] N. Provenza, A. Paulk *et al.*, "Decoding task engagement from distributed network electrophysiology in humans," *Journal of Neural Engineering*, vol. 16, p. 056015, 08 2019.

[13] A. Widge, S. Zorowitz *et al.*, "Deep brain stimulation of the internal capsule enhances human cognitive control and prefrontal cortex function," *Nature Communications*, vol. 10, p. 1536, 04 2019.

[14] A. Bastos and J.-M. Schoffelen, "A tutorial review of functional connectivity analysis methods and their interpretational pitfalls," *Frontiers in Systems Neuroscience*, vol. 9, 01 2016.

[15] R. S. Desikan, F. Segonne *et al.*, "An automated labeling system for subdividing the human cerebral cortex on mri scans into gyral based regions of interest," *NeuroImage*, vol. 31, no. 3, pp. 968 – 980, 2006.

[16] T. Xu, K. R. Cullen *et al.*, "Classification of borderline personality disorder based on spectral power of resting-state fMRI," in *2014 36th Annual International Conference of the IEEE Engineering in Medicine and Biology Society*, 2014, pp. 5036–5039.

[17] K. K. Parhi and Z. Zhang, "Discriminative ratio of spectral power and relative power features derived via frequency-domain model ratio with application to seizure prediction," *IEEE Transactions on Biomedical Circuits and Systems*, vol. 13, no. 4, pp. 645–657, 2019.

[18] Y. Park, L. Luo *et al.*, "Seizure prediction with spectral power of eeg using cost-sensitive support vector machines," *Epilepsia*, vol. 52, no. 10, pp. 1761–1770, 2011. [Online]. Available: https://onlinelibrary.wiley.com/doi/abs/10.1111/j.1528-1167.2011.03138.x

[19] Z. Zhang and K. K. Parhi, "Seizure detection using regression tree based feature selection and polynomial SVM classification," in *2015 37th Annual International Conference of the IEEE Engineering in Medicine and Biology Society (EMBC)*, 2015, pp. 6578–6581.

[20] J. Rouder, P. Speckman *et al.*, "Bayesian t test for accepting and rejecting the null hypothesis," *Psychonomic bulletin & review*, vol. 16, pp. 225–37, 05 2009.

[21] S. Goodman, "A dirty dozen: Twelve p-value misconceptions," *Seminars in Hematology*, vol. 45, no. 3, pp. 135 – 140, 2008, interpretation of Quantitative Research.

[22] C. Keysers, V. Gazzola *et al.*, "Using Bayes factor hypothesis testing in neuroscience to establish evidence of absence," *Nature Neuroscience*, vol. 23, pp. 788–799, 07 2020.

[23] J. F. Cavanagh and M. J. Frank, "Frontal theta as a mechanism for cognitive control," *Trends in Cognitive Sciences*, vol. 18, no. 8, pp. 414 – 421, 2014.

[24] P. S. Cooper, F. Karayanidis *et al.*, "Frontal theta predicts specific cognitive control-induced behavioural changes beyond general reaction time slowing," *NeuroImage*, vol. 189, pp. 130 – 140, 2019.

[25] M. Vaghi, P. Vértes *et al.*, "Specific frontostriatal circuits for impaired cognitive flexibility and goal-directed planning in obsessive-compulsive disorder: Evidence from resting-state functional connectivity," *Biological Psychiatry*, vol. 81, 08 2016.

[26] T. A. Lesh, A. J. Westphal *et al.*, "Proactive and reactive cognitive control and dorsolateral prefrontal cortex dysfunction in first episode schizophrenia," *NeuroImage: Clinical*, vol. 2, pp. 590 – 599, 2013.

[27] N. Metuki, T. Sela *et al.*, "Enhancing cognitive control components of insight problems solving by anodal tDCS of the left dorsolateral prefrontal cortex," *Brain Stimulation*, vol. 5, no. 2, pp. 110 – 115, 2012.

[28] L. Dubreuil-Vall, P. Chau *et al.*, "tDCS to the left DLPFC modulates cognitive and physiological correlates of executive function in a state-dependent manner," *Brain Stimulation*, vol. 12, no. 6, pp. 1456–1463, 2019.